08,09

# Defect structure of the lithium doped nickel oxide

© S.N. Shkerin[1], A.Yu. Nikolaev[1], O.I. Gyrdasova[2], T.A. Kuznetsova[1], A.R. Mullabaev[1], R.K. Abdurakhimova[1], A.V. Kosov[1]

[1] Institute of High-Temperature Electrochemistry, Ural Branch, Russian Academy of Sciences, Yekaterinburg, Russia
[2] Institute of Solid State Chemistry, Russian Academy of Sciences, Ural Branch, Yekaterinburg, Russia

E-mail: shkerin@mail.ru

*Received June 15, 2023*
*Revised June 15, 2023*
*Accepted August 5, 2023*

Solid derivatives $Ni_{1-x}Li_xO \cdot (0 \leq x \leq 0.1)$ were produced by the thermolysis of formate precursor complexes $Ni_{1-x}Li_x(HCOO)_2 \cdot 2H_2O$ at 700°C in air. There are two regions of single phase compositions banded by 4 at.% Li one. X-ray structure is Face Centered Cubic (FCC, Fm3m) for both regions. Experimental molar mass was calculated using a pycnometric density and X-ray data results, taking into consideration chemical composition, determined by isotope method. Structural defects are discussed and application of Raman spectroscopy is pointed to be necessary. Two laser sources (633 and 532 nm) were applied in a temperature region from room temperature up to 700°C. True Stokes lines are distinguished from other Raman lines and they are referred to photoluminescence. After consideration both X-ray and Raman spectroscopy results we concluded that materials structure is fluoride-like ($CaF_2$) with high defect concentration. This structure is stable for compositions with Li concentration more than 4%. Derivatives with Li concentration less than 4% are undergo the transition into the rock salt structure during a high temperature treatment. In contrast with pure cubic NiO its derivatives Ni(Li)O have orthorhombic structure at room temperature.

**Keywords:** Ni(Li)O, pycnometric density, Raman scattering, phase transition.

DOI: 10.61011/PSS.2023.10.57226.113

## 1. Introduction

Although the first studies of nickel oxide doped with lithium oxide Ni(Li)O date refer to 1954 [1], reliable data on the defective structure of these materials cannot be found in the open publications. Paper [2] indicates the presence of nickel cations with different charge states, which is based on the manifestation of the magnetic properties of these oxides. Based on same positions, i.e. coexistence of cations $Ni^{2+}$and $Ni^{3+}$, we study the increase in the electrical conductivity of the material with increase in lithium concentration [3]. The properties are not reproducible [4], which is usually discussed from the point of view of the oxygen activity influence on the ratio of the proportions of nickel cations with different charge states [5,6] and the uncontrolled loss of lithium at elevated temperatures during synthesis [7]. In recent decades the main activity of researchers were aimed at materials with very high lithium concentrations, which correspond to $LiNiO_2$, used as electrode materials for lithium current sources. Only in the last few years the interest in Ni(Li)O arises again due to the application of new low-temperature synthesis methods [8]. This information relates to the properties of Ni(Li)O solid solutions obtained by the method of „soft synthesis“. The comparison of the results on the chemical composition, unit lattice volume and pycnometric density made it possible for the first time to obtain reliable data on the mass of the formula unit, i.e. about the defectiveness of these solid solutions. High-temperature Raman scattering spectroscopy, performed using sources with different wavelengths, made it possible to identify Stokes lines characterizing the structure of the material against the background of photoluminescence bands specific to Ni(Li)O at room temperature.

## 2. Experimental part

### 2.1. Preparation of samples

Eleven samples $Ni_{1-x}Li_xO$ were synthesized with various content of lithium of 0 to 10 mol.% with increment 1 mol.%. Stoichiometric mixtures of nickel carbonate $NiCO_3$ (manufacturer Ural Chemical Plant, reagent grade, GOST 4466-78) and lithium carbonate $Li_2CO_3$ (chemically pure), pre-calcined at 600°C, dissolved in nitric acid until a homogeneous solution was formed, which was evaporated to dry residues of mixed nitrate $Ni(Li)(NO_3)_2$.

Concentrated formic acid was added to the obtained nitrate. The ion exchange reaction occurs rapidly with abundant release of nitrogen oxides. After termination of brown gas release, we obtain a complex with an organic ligand — a complex formate of the composition $Ni_{1-x}Li_x(HCOO)_{2-x}$, which was used as an individual precursor to

obtain the final product. The precursors were annealed in two stages:

— for one hour at 400°C, the decomposition products of the formate group were removed ($H_2O$ and $CO_2$);

— then for 4 h at 700°C the solid solutions of $Ni_{1-x}Li_xO$ were formed.

### 2.2. Determination of lithium concentration

The mass fraction of lithium oxide in samples of the studied ceramic samples NiO-$Li_2O$ was determined by mass spectrometry with inductively coupled plasma on a NexIon 2000 device (Perkin Elmer, USA). A sample weight of powder about 0.1 g was weighed on an analytical balance with an accuracy of 0.0001 g in fluoroplastic beakers 2 $cm^3$ of nitric acid, purified by distillation without boiling, was added to the beaker with sample weight, the beaker was covered with a fluoroplastic lid and heated at a temperature of 150°C until the sample weight was completely dissolved. After which the beaker contents was quantitatively transferred into a measuring bottle with a capacity of 100 $cm^3$. The initial solution was diluted with a 1 wt.% solution of nitric acid to approximate lithium concentration of 50–100 $\mu g/dm^3$ and in mass spectrometer. The calibration characteristic of the spectrometer, expressing the dependence of the magnitude of the analytical signal of the lithium-7 isotope on the mass concentration of lithium, was established using three standard samples for calibration with lithium concentrations of 30, 50 and 120 $\mu g/dm^3$ and three series of measurements. The analysis result was arithmetic average of three parallel measurements.

### 2.3. X-ray study

Certification and monitoring of the phase composition of the samples were carried out by powder X-ray diffraction analysis (XDA) on a Bruker Advance D8 diffractometer in Cu-K$\alpha$-radiation ($\lambda = 1.5406$ A). The samples were scanned at room temperature in air in the range 10–122° with increment $\Delta 2\theta = 0.01°$ at an angular scanning speed of 0.8°/min, the total number of increments was 11000. Analysis of the phase composition and calculation of crystallographic parameters were carried out using the Smart Lab Studio II software package based on database PDF-2 ICDD (Powder Diffraction File PDF2 ICDD Release 2019).

### 2.4. Determination of pycnometric density

Pycnometric density was determined using a helium pycnometer AccuPyc II 1340. Guaranteed reproducibility is ±0.01% of the nominal limit volume, provided that clean, dry, with steady-temperature samples are analyzed using helium in temperature range of 15–35°C. The measurement error is 0.03% of the readings plus 0.03% of the volume of the analysis chamber.

### 2.5. Studies by Raman scattering method

RS studies were carried out using Renishaw U 1000 microscope-spectrometer with two different sources:

– green radiation ($\lambda = 532$ nm); power of Nd : YAG-laser was 50 mW;

– in red radiation ($\lambda = 633$ nm) power of HeNe-laser was 30 mW.

## 3. Results and discussion

Figure 1 shows the example of diffraction pattern, and in Table 1 the results of their calculation are given. With the exception of the sample with a target lithium concentration of 5%, all samples are single-phase, with a cubic structure corresponding to the symmetry group Fm3̄m. The sample with five percent of the target lithium concentration contains a second phase — metal nickel.

Figure 2, *a* shows the experimentally determined concentrations of lithium oxide in the samples. The results obtained allow us to speak about two different solid solutions. The

**Table 1.** Results of X-ray diffraction patterns processing

| № | $a$ | $\Delta a$ | $R_{wp}$, % | $R_p$, % | $S$ | $\chi^2$ |
|---|---|---|---|---|---|---|
| 0 | 4.17832 | 1.8E-5 | 3.57 | 2.74 | 1.7813 | 3.1729 |
| 1 | 4.17793 | 1.9E-5 | 4.26 | 3.05 | 2.1846 | 4.7724 |
| 2 | 4.17666 | 8E-6 | 3.73 | 2.79 | 1.9254 | 3.707 |
| 3 | 4.17571 | 1.1E-6 | 3.69 | 2.78 | 1.8807 | 3.537 |
| 4 | 4.17465 | 7E-6 | 3.98 | 2.95 | 2.0503 | 4.2038 |
| 6 | 4.16889 | 1.2E-5 | 3.71 | 2.82 | 1.8633 | 3.4719 |
| 7 | 4.16783 | 1.3E-5 | 3.87 | 2.93 | 1.9034 | 3.6229 |
| 8 | 4.16605 | 3E-5 | 3.88 | 2.99 | 1.9658 | 3.8644 |
| 9 | 4.16399 | 3E-5 | 4.13 | 3.1 | 2.0446 | 4.1803 |
| 10 | 4.16381 | 2E-5 | 3.77 | 2.9 | 1.8777 | 3.5259 |

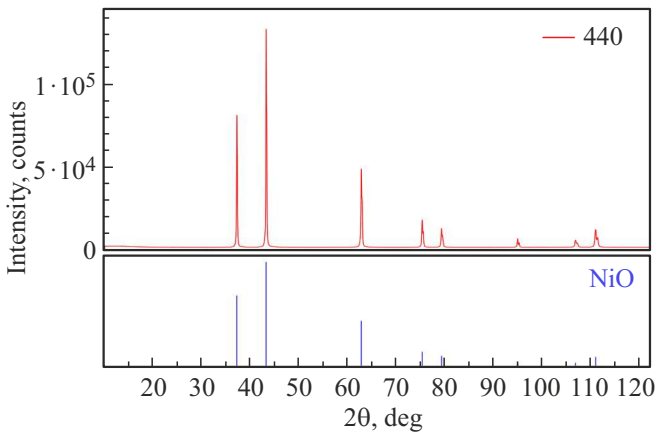


**Figure 1.** Example of diffraction pattern

lithium concentrations in nickel oxide were recalculated from the results of Figure 2, *a* and presented in Figure 2, *b* as the fraction of lithium in the material under study. For the composition with highest lithium content, the target concentration of which was set as 10%, actually it was 8.4. This reflects the lithium carryover during synthesis. The amount of lithium lost differs for two different regions of solid solutions (Figure 2, *b*). The composition separating the two solid solutions, and corresponding to the target lithium content 5% after correction for carryover contains about 4%.

Figure 3 shows the constants of lattice with cubic structure depending on the lithium concentration. For the range of compositions with concentration of lithium cations less than 4% (for $Li_2O$ corresponds to 2%), the dependence of the lattice constant on the composition is close to linear, which is typical for solutions. For the range of compositions with lithium cations concentration of more than 4%, a complex dependence is observed, similar to a step.

Figure 4 shows the pycnometric density for single-phase samples. Since, as described in the experimental part, the measurement error is calculated taking into account the free

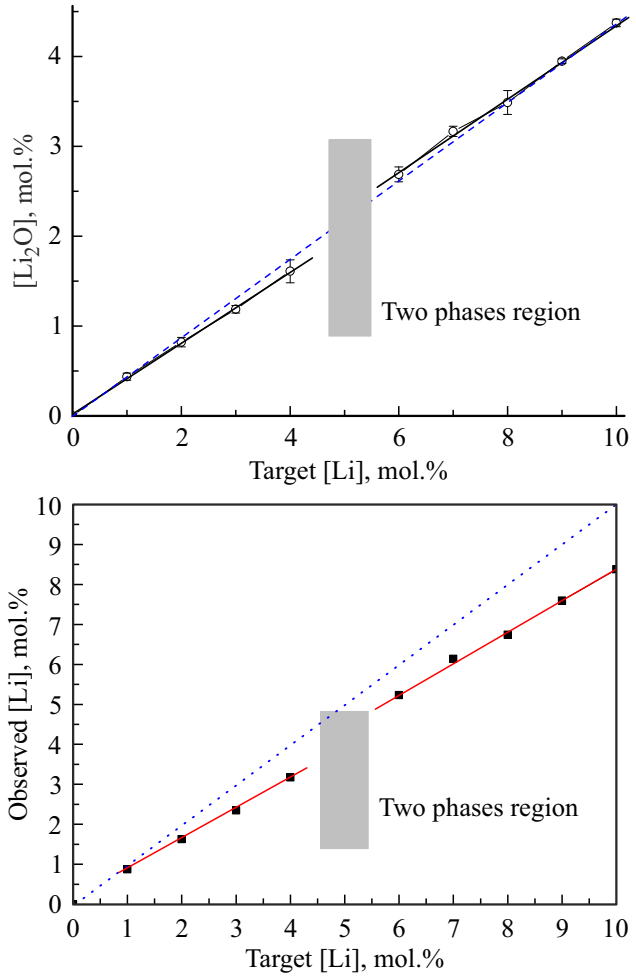


**Figure 2.** The experimentally determined concentration of lithium oxide $Li_2O$ (top) and lithium concentration Ni(Li)O (bottom) depending on the target concentration.

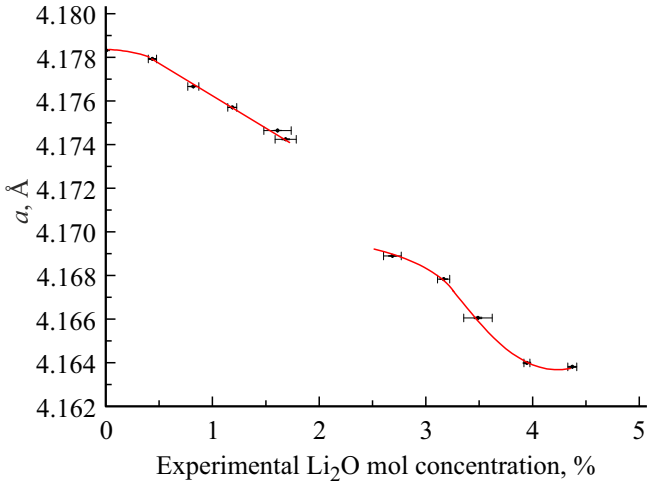


**Figure 3.** Constant of lattice with cubic structure with symmetry group Fm3m vs. concentration of lithium oxide.

**Table 2.** Determination of pycnometric density of system NiO-Li

| № | Composition of sample | Pycnometric densoty, g/cm$^3$ | Volume, cm$^3$ |
|---|---|---|---|
| 1 | NiO | 6.6843 ± 0.0012 | 0.2053 ± 0.0004 |
| 2 | NiO−1% Li | 6.7105 ± 0.0069 | 0.1222 ± 0.0001 |
| 3 | NiO−2% Li | 6.7530 ± 0.0042 | 0.0689 ± 0.0001 |
| 4 | NiO−3% Li | 6.8664 ± 0.0122 | 0.0544 ± 0.0001 |
| 5 | NiO−4% Li | 6.9614 ± 0.0345 | 0.0316 ± 0.0002 |
| 7 | NiO−6% Li | 6.6326 ± 0.0060 | 0.1646 ± 0.0001 |
| 8 | NiO−7% Li | 6.5690 ± 0.0042 | 0.2287 ± 0.0001 |
| 9 | NiO−8% Li | 6.5489 ± 0.0040 | 0.1523 ± 0.0001 |
| 10 | NiO−9% Li | 6.4712 ± 0.0028 | 0.3356 ± 0.0001 |
| 11 | NiO−10% Li | 6.4221 ± 0.0068 | 0.2398 ± 0.0003 |

volume of the chamber, a set of results is also presented in Table 2. The squares in Figure 4 represent literature data from two different sources for undoped nickel oxide. Our results are in good agreement with them. From Figure 4, the multidirectional behavior of the dependences of density on lithium concentration for different regions of the solid solution is obvious.

Since the pycnometric density of a single-phase material is free from contributions from three-dimensional (pores in ceramics, second phases) and two-dimensional (ceramic grain boundaries) defects, it is possible to calculate the mass of the formula unit reflecting the contribution of defects with a smaller size, primarily point ones (Figure 5).

When calculating the mass of the formula unit, we are based on the

– known density (Figure 4),

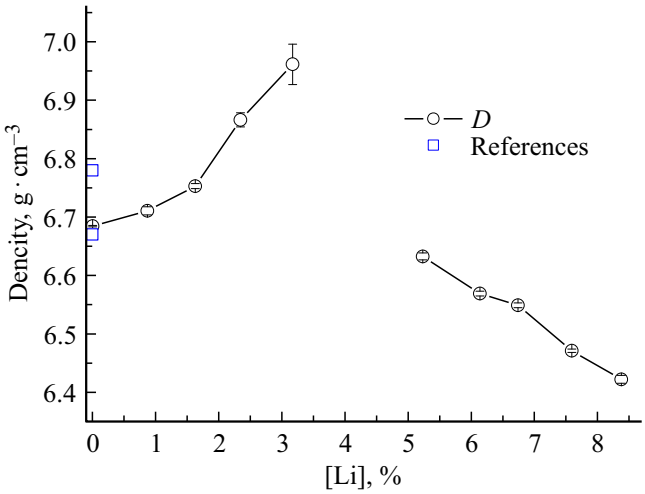


**Figure 4.** Pycnometric density of Ni(Li)O vs. lithium concentration.

– volume of lattice cell equal to cube of lattice constant from Figure 3,

– understanding that lattice cell is formed by four formula units.

The horizontal dashed line in Figure 5 represents the mass of defect-free nickel oxide (74.699 g/mol). The mass for undoped nickel oxide turned out to be lower (73.4343 g/mol, shown by arrows), which indicates the vacancies presence in the resulting material. If we assume that these vacancies are only oxygen vacancies, then they constitute 7.9% of the total number of oxygen positions. A similar approach for the concentration estimation of absolutely dominant cation vacancies gives 2.1%.

In the publications, the most popular representations of the defect structure of Ni(Li)O are based on the reaction

$$2Ni^{2+} \Longrightarrow Ni^{3+} + Li^{+}, \qquad (1)$$

going without oxygen exchange. It is justified by magnetic and electrical properties described by the coexistence of nickel cations in different charge states. In this case the change in mass upon the lithium introduction is described by $-\Delta\mathbf{m} = \mathbf{m}_{Ni} - \mathbf{m}_{Li}$. This behavior corresponds to straight line *1* in Figure 5. Obviously, it also differs from the observed experimental dependence.

An alternative, but also popular, approach is to consider the formation of oxygen vacancies

$$Ni^{2+} \Longrightarrow Li^{+}_{Ni} + 1/2V_O. \qquad (2)$$

In this case the change in mass upon the lithium introduction is described as follows

$$-\Delta\mathbf{m} = (\mathbf{m}_{Ni} - \mathbf{m}_{Li}) + 1/2\mathbf{m}_O.$$

This behavior corresponds to straight line *2* in Figure 5. Obviously it also differs from the observed dependence that steadily rises. The increasing behavior of the observed mass of the formula unit can be described through the mechanism of vacancies destruction during the lithium introduction. Straight line *3* in Figure 5 corresponds to the slope

$$\Delta\mathbf{m} = (\mathbf{m}_{Ni} + \mathbf{m}_O) + (\mathbf{m}_{Li} + 1/2\mathbf{m}_O), \qquad (3)$$

when the introduction of 1/2 ($Li_2O$) makes the existence of one more anion and cation vacancies energetically unfavorable. The increasing course of the experimental curve is nonlinear, which implies more complex mechanisms for the defects formation or destruction than the mechanism presented by straight line *3*. But such a large slope and its sign force us to consider specifically the mechanisms of filling cation vacancies.

What stands out is the right side of Figure 5, corresponding to the second solid solution — it is described by straight line. The change in mass for this section of the experimental dependence can be described as

$$-\Delta\mathbf{m} = \left((\mathbf{m}_{Ni} - \mathbf{m}_{Li}) + 1/2\mathbf{m}_O\right) + (\mathbf{m}_{Ni} + \mathbf{m}_O), \qquad (4)$$

which corresponds to the oxygen vacancy formation according to mechanism (2), coupled with the forced formation of one vacancy in both the cation and anion sublattices. The correspondence between the experimental results and the model (4) indicates that it is, apparently, being implemented.

Besides, in Figure 5 the attention is drawn to the presence of points located above the straight line of defect-free nickel oxide. This may indicate the presence of interstitial cations. This assumption can be confirmed by vibrational spectroscopy methods. In the case of materials based on nickel oxide, this is a difficult task, since the Raman spectra obtained in sources with different wavelengths do not coincide, which indicates a significant contribution of photoluminescence. Similar effects were recently examined in detail for materials with a fluorite structure [9,10]. You can exclude the influence of photoluminescence caused by defects by increasing the temperature, as a result of

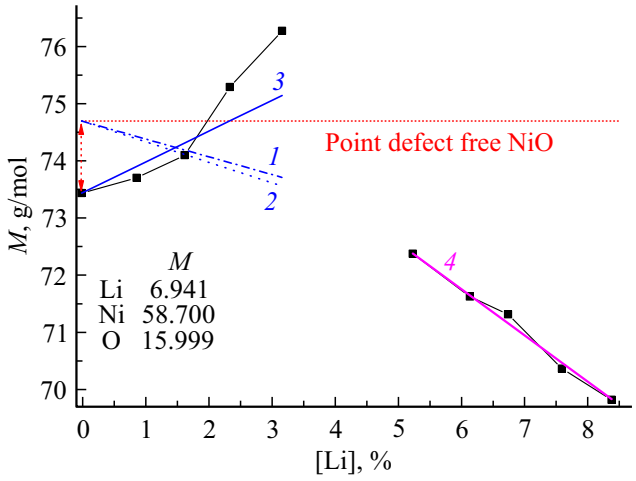


**Figure 5.** Mass of formula unit vs. amount of lithium introduced. Horizontal line — mass of defect-free nickel oxide, *1–4* mass change within different models.

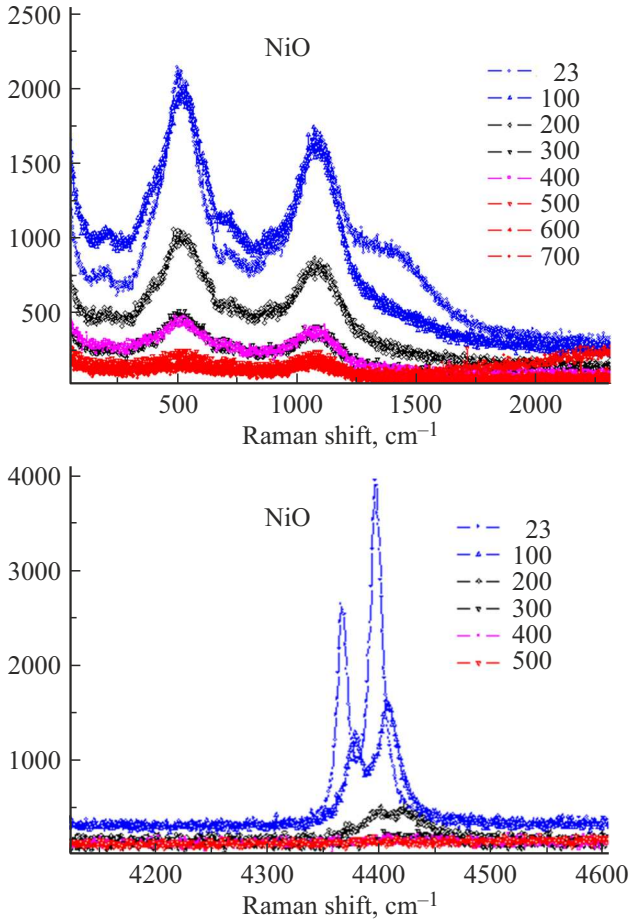


**Figure 6.** Raman spectra obtained at excitation wavelength of 532 nm and various temperatures.

this they disappear. Stokes lines can be separated from photoluminescence lines by their independence from the wavelength of the radiation used. In connection with this, we carried out studies using Raman scattering during temperature increasing, and for a number of compositions using two different lasers. Figure 6 shows the Raman spectra for undoped nickel oxide using a green laser. What stands out is that upon temperature changes from room temperature (23°C) to 400°C in Figure 6, *a* a number of bands disappear.

Figure 6, *b* shows photoluminescence lines in the region of large wave numbers, observed for all images. As the temperature rises, their frequencies shift to long wavelength region, and the intensity decreases until disappearance. This is a typical example for photoluminescence of defects, such as oxygen vacancies. Exactly the lines were previously reported in [10].

Figures 7 and 8 compare Raman spectra using two different sources. It is clearly visible that only one, rather wide line, near 480 $cm^{-1}$ is Stokes line. Such spectrum is typical for the structure of fluorite [11], but not for rock salt, where a pair of lines 184 and 275 $cm^{-1}$ [12] is typical.

Both the fluorite structure and the rock salt structure are cubic, with symmetry group $Fm\bar{3}m$. They have the same cation basis: (0, 0, 0), (1/2, 0, 0), (0, 1/2, 0), (0, 0, 1/2). Specifically it determines X-ray diffraction. As a consequence, there are problems to separate these two structures by X-ray diffraction.

But for these two structures the anions basis is significantly different. The structure of rock salt is characterized by four positions of anions, and the structure of fluorite is characterized by eight positions. The coordination number of the cation in the structure of rock salt is — 6, in the structure of fluorite — 8.

Based on the results in Figures 7 and 8, the studied samples, including undoped nickel oxide, have fluorite structure but not rock salt structure, as it is usually discussed. As result of this new knowledge, the results in Figure 5 should be compared not with the straight line for defect-free nickel oxide, but with the straight line for a hypothetical nickel oxide with fluorite structure (90.69 g/mol), which eliminates the question of interstitial cations. At the same time, the defectiveness of the lattice would be unacceptably high if we considered the entire lattice as having fluorite structure. Apparently, we are talking about cationic framework with the basis described above and the symmetry group $Fm\bar{3}m$,

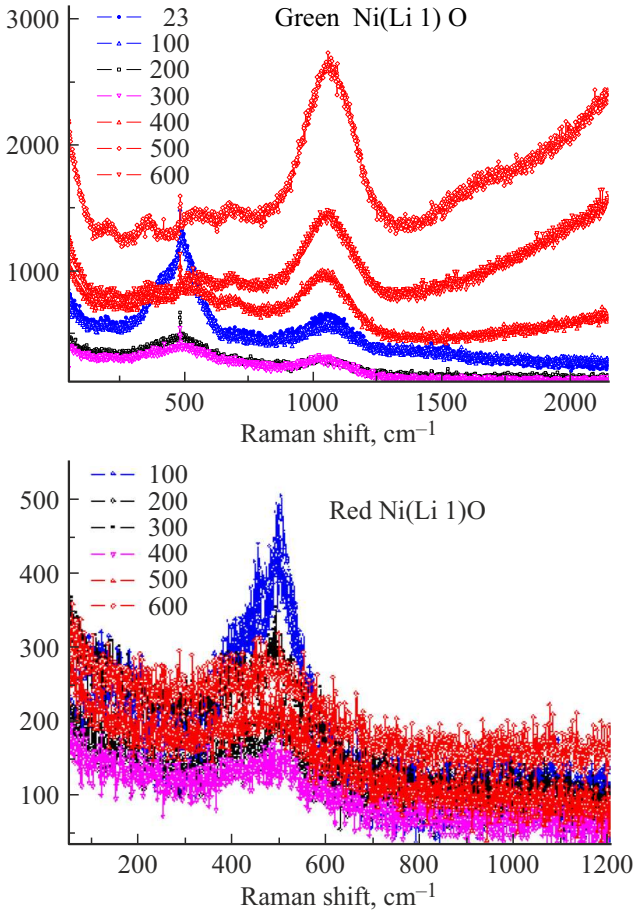


**Figure 7.** Raman spectra obtained at various temperatures. A — using green (532 nm), B — red (633 nm) sources.

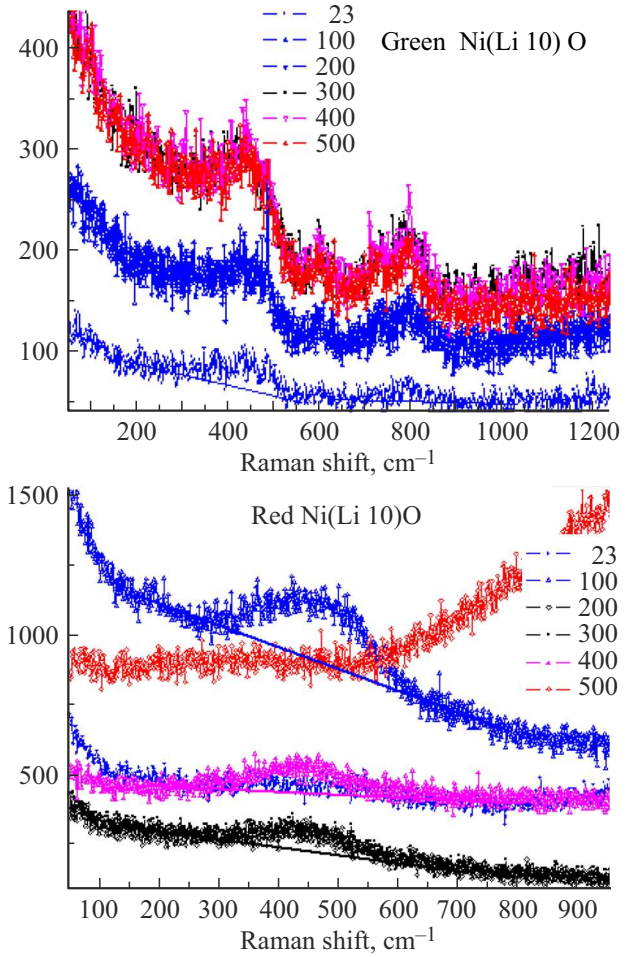


**Figure 8.** Raman spectra obtained at various temperatures. A — using green (532 nm), B — red (633 nm) sources.

within which there is anions redistribution. Exposure of samples for 150 h at 850°C leads not only to the loss of part of the lithium by the samples, but also to change in the structure for solid solutions with low lithium content. Their structure at room temperature becomes rhombohedral ($R\bar{3}m$, PDF Card 00-044-1159, 1992). It is characterized by a coordination number 6, i. e. matches the structure of rock salt, although distorted. The symmetry of samples for solid solutions with high lithium content does not change and remains cubic, with symmetry group $Fm\bar{3}m$.

Based on the totality of the results obtained, we can conclude that phase transition exists in Ni(Li)O solid solutions. At low lithium concentrations, up to 4 mol percent, the rock salt structure is stable, which coincides with the data for undoped nickel oxide. Its formation occurs through the formation of fluorite-type structure, which is metastable for this range of compositions, but specifically it is initially obtained using soft synthesis methods. Unlike undoped nickel oxide, which is cubic at room temperature, solid solutions based on it have rhombohedral distortions at room temperature.

Solid solutions with lithium concentration greater than 4% are characterized by the stable fluorite structure.

## 4. Conclusion

The thermolysis in air at 700°C of formate precursor complexes $Ni_{1-x}Li_x(HCOO)_2 \cdot 2H2O$ produces appropriate solid solution $Ni_{1-x}Li_xO \cdot (0 \leq x \leq 0.1)$. With the exception of one composition (about four mole percent of lithium), all samples are single-phase. The presence of two regions with various properties of solid solutions with an FCC structure ($Fm\bar{3}m$), separated by this lithium concentration, is shown.

Study of

a) the actual composition of the synthesized samples,

b) phase composition and lattice constants, including the volume of the lattice cell,

c) pycnometric density

made it possible to determine the mass of the formula unit and its dependence on lithium concentration. The change in the mass of the formula unit with change in lithium concentration differs significantly from the models available in the publications (*1* and *2* in Figure 5):

1) changes occur much faster than it follows from existing models and, in some cases, have the opposite sign;

2) for solid solutions with low lithium concentrations, the mass of the formula unit increases, and for a number of compositions it is even higher than the mass of defect-free nickel oxide. This rises the question of the interstitial cations existence, which was verified using the Raman scattering method.

Studies by Raman spectroscopy using two different sources (633 and 532 nm) in the temperature range from room temperature to 700°C made it possible to isolate from the totality of all reflections, most of which are due to photoluminescence, one very broad line near 480 $cm^{-1}$, which is Stokes line. This spectrum is typical for the structure of fluorite, but not of rock salt, which excludes the question of the interstitial cations existence.

Long-term annealing at elevated temperature does not change the symmetry of the lattice of solid solutions with lithium concentration greater than 4%; it remains cubic, like fluorite. For solid solutions with low lithium concentrations, the lattice symmetry decreases to rhombohedral, which corresponds to the structure of rock salt with corresponding distortions. Based on the totality of the results obtained, we can conclude that phase transition exists in Ni(Li)O solid solutions. At low lithium concentrations, up to 4 mol percent, the rock salt structure is stable. Its formation occurs through the formation of fluorite-type structure, which is metastable for this range of compositions, but specifically it is initially obtained using soft synthesis methods. Solid solutions with lithium concentration greater than 4% are characterized by the stable fluorite structure.

### Acknowledgments

The study was performed using the equipment at the Shared Access Center of the Institute of High Temperature Electrochemistry of the Ural Branch of RAS.

### Conflict of interest

The authors declare that they have no conflict of interest.

## References

[1] P.I. Fensham. J. Am. Chem. Soc. **76**, *3*, 969 (1954).
[2] J Goodenough, D. Wickham, W.J. Croft. J. Phys. Chem. Solids **5**, 107 (1958).
[3] G.K. Stepanov, A.M. Trunov. Izv. AN SSSR **6**, 67 (1961). (in Russian).
[4] J. Deren, M. Rekas. Roczniki Chem. Ann. Soc. Chim. Polonorum. **46**, 1411 (1972).
[5] H. Migeon, M. Zanne, C. Gleitzer, J. Aubry. J. Mater. Sci. **13**, 461 (1978).
[6] J. Deren, M. Rekas, G. Rog. Roczniki Chem. Ann. Soc. Chim. Polonorum. **46**, 1837 (1972).
[7] E. McCalla, G.H. Carey, J.R. Dahn. Solid State Ionics **219**, 11 (2012).
[8] A. Bhatt, R. Ranjitha, M. Santosh, C. Ravikumar, S. Prashantha, R. Maphanga, G. de Silva. Materials **13**, 2961 (2020). DOI: 10.3390/ma13132961
[9] S.N. Shkerin, E.S. Yulyanova, E.G. Vovkotrub. Neorgan. materialy **57**, *11*, 1213 (2021). (in Russian).
[10] S.N. Shkerin, A.N. Meshcherskikh, T.V. Yaroslavtseva, R.K. Abdurakhimova. FTT **64**, *12*, 1985 (2022). (in Russian).
[11] V.G. Keramidas, W.B. White. J. Chem. Phys. **59**, *3*, 1561 (1973).
[12] R.S. Krishnan. Proc. Royal Soc. London. Ser. A **187**, *1009*, 188 (1946).

*Translated by I.Mazurov*